# Fabrication of Ultrafiltration Membrane with Antibacterial Properties by Blending Ag/UiO-66-NH<sub>2</sub> and Bamboo Cellulose

Rengui Weng,<sup>a,b,\*</sup> Shuo Dong,<sup>b</sup> Feng Tian,<sup>b</sup> Dongqi Liao,<sup>b</sup> Jie Qin,<sup>b</sup> Junjiang Bai,<sup>b</sup> Guohong Chen,<sup>b</sup> Shaojie Li,<sup>b</sup> and Shikang Zhao <sup>b</sup>

Cellulose is a widely available organic substance that forms membranes with excellent hydrophilicity and biocompatibility. However, it is prone to biological contamination because its surface is conducive towards the accumulation of biologically active substances, which has hindered its application potential. In this work, an antimicrobial cellulose-based membrane (Ag/UiO-66-NH<sub>2</sub>@BCM) with high water flux, high retention rate, and good hydrophilicity was prepared. At an optimal blend ratio of 1 wt% Ag/UiO-66-NH<sub>2</sub>, the membrane exhibited significant improvements, including a 31% increase in pure water flux, a Bovine Serum Albumin retention rate of 99.6%, and a water flux recovery of 97.4%. Crucially, the membrane demonstrated potent antibacterial, showcasing its broadspectrum antimicrobial properties. Investigations into the ability of Ag/UiO-66-NH<sub>2</sub>@BCM to remove Pb<sup>2+</sup>, Cd<sup>2+</sup>, and Cr<sup>6+</sup> ions from a water column revealed that the maximum adsorption capacity of the monolayer was 405, 390, and 328 mg/g, respectively. The composite membrane demonstrated broad-spectrum and highly effective antimicrobial properties, along with efficient removal of heavy metal ions. The proposed method can be utilized to prepare other composite membranes for water treatment and other fields of membrane separation technology.

DOI: 10.15376/biores.19.4.8988-9006

Keywords: Cellulose membrane; Membrane separation; Antibacterial property; Adsorption property

Contact information: a: Institute of Biology and Chemistry, Fujian University of Technology, Fuzhou 350118, China; b: College of Ecological Environment and Urban Construction, Fujian University of Technology, Fuzhou 350118, China; \*Corresponding author: wengrengui109@fjut.edu.cn

#### INTRODUCTION

The demand for water purification has surged globally and in China due to the rapid advancement of living standards. Among the many water purification technologies currently implemented, membrane-based technology has emerged as a pivotal player (Khanzada *et al.* 2020; Peydayesh and Mezzenga 2021; Tarpeh and Chen 2021). Various membrane methods, such as microfiltration (MF), ultrafiltration (UF), nanofiltration (NF), reverse osmosis (RO), and membrane distillation (MD), have been employed for water treatment purposes (Aloulou *et al.* 2021; Fatima *et al.* 2021; Huang *et al.* 2021; Jawad *et al.* 2021; Weng *et al.* 2021, 2022; Kaur *et al.* 2022; Wu *et al.* 2022). At present, UF technology stands as one of the most widely adopted methods in wastewater treatment (Ajibade *et al.* 2021; Awad *et al.* 2021; Huang *et al.* 2021; Zhang 2022). UF membranes are characterized by their remarkable water permeability, suitable selectivity, and effective antifouling properties, which are largely influenced by the membrane material itself.

Among the various UF membranes, natural bamboo cellulose (BC) presents several unique advantages, such as good regenerability, wide availability, affordability, and biodegradability. Additionally, it can be modified with relatively facile methods and possesses high tensile strength. Due to its short growth cycle and robust renewability, BC ranks as one of China's most vital forest resources, second only to wood. The chemical composition of BC closely resembles that of wood, primarily comprising lignin, cellulose, and hemicellulose (Zhao et al. 2021; Zou et al. 2022; Janmohammadi et al. 2023). With the diminishing availability of wood resources, there is an urgent need to promote the sustainable and harmonious development of the economy and environment. In this regard, bamboo could be a promising alternative for wood, offering great potential for mitigating the ecological imbalances that stem from the excessive use of wood. Consequently, the development of composite membranes utilizing BC as the primary raw material offers an eco-friendly and cost-effective solution. However, cellulose membranes are susceptible to protein fouling in aqueous environments due to the partially hydrophobic nature and low surface energy of cellulose, depending on its crystal orientation (Yamane et al. 2006). The adhesion of polysaccharides or other organic contaminants can lead to pore blockages and a decline in flux, ultimately impacting the operational longevity of the membrane. This drawback of membrane biofouling has hindered the widespread adoption of cellulose membranes. To enhance membrane performance, several modification strategies have been explored, including chemical grafting, surface modification, irradiation, and blending techniques. Notably, the blending approach with hydrophilic materials has garnered considerable attention owing to its simplicity and mild processing conditions. Over the past decade, this method has demonstrated the amalgamation of the benefits of the polymer matrix and the filler material, thereby augmenting the overall properties of the membrane.

Antibacterial membranes have been developed by incorporating a variety of materials. For instance, Zhang *et al.* (2019) introduced a pioneering approach to fabricate antibacterial guanidyl-functionalized graphene/polysulfone mixed matrix UF membranes using a non-solvent induced phase separation method (Zhang *et al.* 2019). The mixed matrix membranes comprising graphene and polysulfone demonstrated remarkable permeability and exceptional antifouling properties when exposed to bovine serum albumin (BSA). Additionally, the membranes exhibited impressive antimicrobial effectiveness over extended durations against both *Escherichia coli* and *Staphylococcus aureus*. In another study, Weng *et al.* (2016) employed N-aminoethyl piperazine propane sulfonate as the monomer in a reaction with 1,3,5-benzenetricarbonyl trichloride to form zwitterionic polyamide membranes, which substantially reduced bacterial adhesion compared to primary membrane.

Certain organic materials indirectly enhance antibacterial performance by modifying the physicochemical properties of the membrane such as hydrophilicity, surface roughness, and charge characteristics. The bacteria are not directly killed; with an increase in operation time, there is a likelihood of accumulation on the membrane surface. In contrast, some studies have demonstrated that inorganic materials, such as metal particles and metal oxides, directly inactivate bacteria through physical damage and the generation of reactive oxygen species. For instance, Zhang *et al.* (2018) developed a series of innovative UF membranes by incorporating copper nanoparticles using an immersion precipitation phase conversion method. When the concentration of copper nanoparticles was 0.4 wt.%, the UF membrane demonstrated an impressive pure water flux of 193 LMH and a notable antibacterial efficacy of 78.9%. In another study, Geng *et al.* (2021) employed zeolitic imidazole framework-8 decorated with graphene oxide (ZGO) as an

antibacterial agent and the modified sample was subsequently integrated into a polyethersulfone matrix to manufacture UF hollow fiber membranes through a phase inversion process. A peak water flux of 95.49 LMH was obtained when the ZGO content was optimized at 1.0 wt%. This composite membrane exhibited significant antibacterial activity against both *Escherichia coli* and *Staphylococcus aureus*, with antibacterial efficiencies of 81.1% and 85.7%, respectively. Despite the enhanced antibacterial attributes of inorganic particles, their compatibility with organic membranes remains challenging, often leading to substantial leakage issues. Consequently, there is substantial research directed towards exploration of antibacterial materials that can maintain stability within organic membranes. Recent investigations have demonstrated that a feasible approach involves the modification of inorganic antibacterial agents with organic materials, thereby enhancing membrane stability without compromising antibacterial properties (Chai *et al.* 2022).

Metal-organic frameworks (MOFs) are intricate three-dimensional crystalline materials formed through the self-assembly of metal clusters and organic ligands via coordination bonds. In recent years, highly stable MOFs such as UiO, MIL, ZIF, and HKUST have found widespread applications (Musarurwa and Tavengwa 2022). Due to their porous nature, high specific surface area, and crystallinity, MOFs have been extensively utilized in the fields of adsorption, catalysis, gas storage, and separation. Notably, MOFs and composite MOF materials have garnered considerable attention in the area of environmental research. Numerous studies have demonstrated that MOF materials can efficiently remove various waterborne pollutants, such as dyes, heavy metals, and aromatic hydrocarbons, primarily through adsorption mechanisms (Miao *et al.* 2022). The porous structure of MOFs allows for precise control over the release of antibacterial ions. The structures and composition of MOFs can be optimized to tailor the release rate of antibacterial ions and resulting antibacterial activity.

Among the various antibacterial agents, silver nanoparticles (Ag NPs), commonly synthesized through a simple reduction reaction, are frequently employed in research due to their excellent antibacterial properties. However, several challenges have hindered the practical applications of pure Ag materials as membrane antibacterial agents. The external conditions of the reduction process such as temperature, illumination, and reaction time are difficult to control, impacting the yield and quality of Ag NPs. This results in high synthesis costs as silver reagents are expensive. Furthermore, reductants like borohydride, dimethylformamide, and thiol can generate numerous by-products, raising material costs and necessitating extensive post-treatment while posing ecological risks and threats to human health. Kim et al. addressed these issues by preparing Ag NPs with improved yield and purity using Laminaria japonica algal extract (Kim et al. 2018). However, the repulsion between pure inorganic particles and organic membranes is undesirable and must be considered in practical applications. Poor compatibility and non-uniform distribution of Ag NPs within polyamide (PA) layers often leads to premature leakage, significantly compromising membrane stability and antibacterial performance. The distinctive skeletal structure of MOFs enhances the stability of silver materials, thereby reducing reagent costs and post-processing burdens.

In this study, zirconium (Zr) was selected as a key element due to its low toxicity and widespread use in dental materials. UiO-66, a chemically and thermally stable MOF was selected due to its excellent chemical and thermal stability. A modified version, UiO-66-NH<sub>2</sub>, sharing structural similarities with UiO-66, had previously demonstrated peroxidase activity and excellent hydrophilic characteristics (Zhang *et al.* 2021). In this

study, a composite material was developed by integrating in-house developed Ag/UiO-66-NH<sub>2</sub> into BC to fabricate a MOF/cellulose UF membrane (Ag/UiO-66-NH<sub>2</sub>@BCM) through immersion precipitation phase conversion. This composite exhibited enhanced permeability, protein retention capacity, and remarkable antibacterial properties. This study investigates the essential physical attributes, surface morphology, crystalline structure, chemical composition, and antibacterial characteristics of Ag/UiO-66-NH<sub>2</sub>@BCM.

#### **EXPERIMENTAL**

#### **Materials and Chemicals**

BC (≥97%) was obtained from Fujian Shaowu Zhongzhu Paper Co. Ltd. ZrC14, DMF(AR, ≥99.5%), H<sub>2</sub>BDC-NH<sub>2</sub>, NaOH, H<sub>2</sub>SO<sub>4</sub>, Cr<sup>6+</sup> standard solution, Pb standard solution, and Cd standard solution were purchased from Aladdin Biochemical Co. Ltd. (Shanghai China). Methanol and AgNO<sub>3</sub> were procured from Nanjing Chemical Reagent Co. Ltd. (Nanjing China). Propyl gallate (CP, ≥99.5%) was obtained from Sinopharm Chemical Reagent Co. Ltd. (Shanghai China). N-methylmorpholine-N-oxide (NMMO) solid powder (≥97%) was purchased from Hainachuan Technology Development Co. Ltd. (Tianjin, China). Bovine serum albumin (BSA, 68 kDa) was procured from Pu Bo Xin Biotechnology Co. Ltd. (Beijing, China).

## Fabrication of the Ag/UiO-66-NH<sub>2</sub>@BCM

Bamboo cellulose membranes (BCMs) were synthesized through the immersion precipitation phase conversion method. The Ag/UiO-66-NH<sub>2</sub> composite material was prepared using a solvothermal approach based on established protocols (Ruan *et al.* 2022). Bamboo pulp boards were first pulverized for 3 min and were then set aside. The synthesis process of Ag/UiO-66-NH<sub>2</sub>@BCMs is depicted in Fig. 1. NMMO (40 g) was initially blended with deionized water (8 g) in a three-necked flask and then heated in an oil bath at 90 °C. Upon complete dissolution of the NMMO, 0.2% propyl gallate was incorporated into the solution as an antioxidant. Following this, BC and Ag/UiO-66-NH<sub>2</sub> were consecutively introduced into the aqueous NMMO solution according to the proportions outlined in Table 1. The temperature was subsequently reduced to 90 °C, the mixer was deactivated, and the mixture was left undisturbed for 5 h to eliminate air bubbles. The NMMO solution was uniformly applied to the surface of a glass plate and then immersed in deionized water for 48 h for the reverse-phase process. Finally, the material was air-dried in a fume hood on the plate to yield Ag/UiO-66-NH<sub>2</sub>@BCMs.

Table 1.	Compo	osition	of B	C and A	Ag/UIO-	-66-NH <sub>2</sub> I	olends

Membrane Code	NMMO (g)	H <sub>2</sub> O BC Ag/UiO (g) (w		Ag/UiO-66-NH <sub>2</sub> (wt%)	BC to Ag/UiO-66-NH <sub>2</sub> Ratio
MO	40	8	1.5	0	1:0
M1	40	8	1.5	0.5	15:1
M2	40	8	1.5	1	7.5:1
M3	40	8	1.5	1.5	5:1

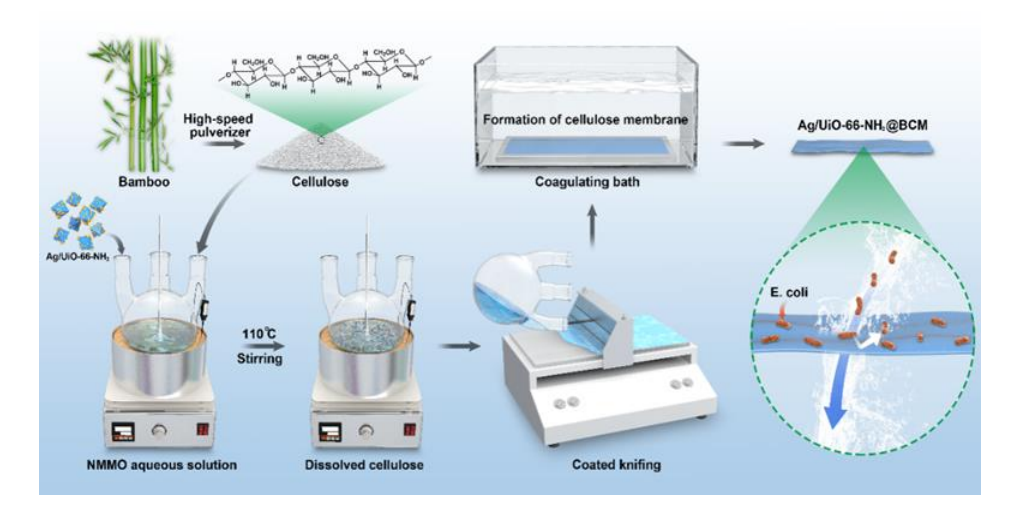


Fig. 1. Preparation of cellulose composite membranes

#### **Characterizations**

Morphology

The surface and cross-sectional morphologies of BCM and 1 wt% Ag/UiO-66-NH<sub>2</sub>@BCM were examined using field emission scanning electron microscopy (FE-SEM, JM-7600F, JEOL Co. Ltd., Japan). Energy dispersive spectroscopy (EDS) was employed to analyze the elemental compositions of these membranes. The composition of BC, Ag/UiO-66-NH<sub>2</sub>, BCM, and Ag/UiO-66-NH<sub>2</sub>@BCM samples was assessed using an X-ray diffractometer (XRD, D8, Bruker AXS Co., Germany).

## Physicochemical structure

The chemical compositions of functional groups of BC, BCM and Ag/UiO-66-NH<sub>2</sub>@BCM samples were analyzed by Fourier transform infrared spectroscopy (FT-IR, Nicolet-460, Bruker Co., Germany). Thermogravimetric tests (TG, Q500, TA Co, USA) were performed to analyze the thermal stability properties of BC, BCM, and Ag/UiO-66-NH<sub>2</sub>@BCM samples.

#### Water permeability performance and ultrafiltration

The determination of pure water flux for the membranes was conducted, employing a custom-designed testing apparatus that could assess separation membrane performance (Membrane filtration system, KCT-PB/785, Xiamen Kaichengtong Machinery Equipment Co., China). The membranes were subjected to preliminary treatment under room temperature and a pressure of 0.1 MPa pressure for 30 min in order to stabilize the pressure and water output. Subsequently, the measurement of water passing through the membrane was carried out at regular intervals every 3 min. The osmotic flux  $Q_{\rm W1}$  ( $Q_{\rm B}$ ) (LMH) of pure water (BSA solution) was calculated from the following equation,

$$Q_{W1}(Q_{\rm B}) = \frac{V}{4r} \tag{1}$$

where  $Q_{W1}$  and  $Q_B$  are the pure water flux of the membrane and the BSA flux of the membrane (LMH), respectively, V is the volume of permeate (L), A is the effective area of the membrane (m<sup>2</sup>), and t is the collection time of permeation (h). The water flux, retention and recovery of the cellulose membrane were measured using a filtration unit, as shown in Fig. 2.

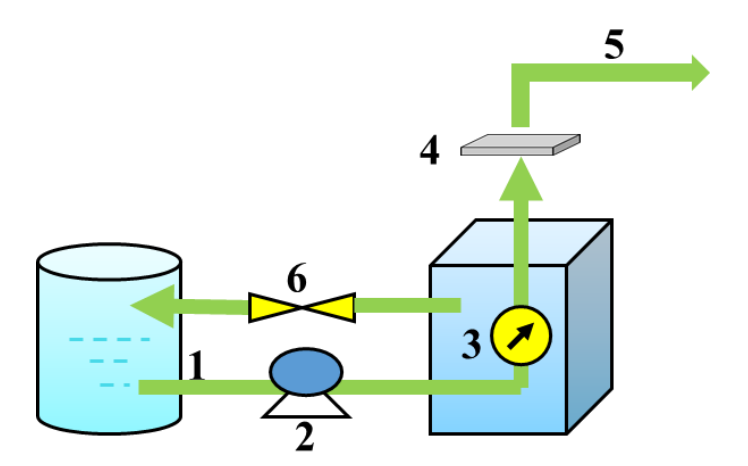


**Fig. 2.** Membrane filtration system: (1) feed port; (2) pump; (3) pressure gauge; (4) cellulose membrane; (5) discharge port; (6) valve

Contact angle was measured using a contact angle meter (DSA25, Dongguan Bolaide Co. Ltd., China) in order to ascertain the hydrophilicity of the membrane. A membrane designated for testing was precisely cut to the required dimensions and affixed to a glass slide. Subsequently, 3  $\mu$ L of distilled water was gently deposited onto the surface of the membrane. Photographs and measurements were obtained at five different locations on each membrane to minimize experimental error. Based on the measurements, the contact angle, which is the angle formed between the water droplet and the membrane surface, was determined. Note that a smaller contact angle corresponds to a higher level of hydrophilicity exhibited by the membrane.

UF experiments were performed on cellulose membranes using BSA as a contaminant. First, a solution of BSA with a mass concentration of 1000 mg/L was prepared. A standard curve was then generated for BSA at a measurement wavelength of 280 mm. In the filtration device, pure water was replaced with BSA solution of 1000 mg/L concentration, and the membrane was placed in the filtration device. The membrane retention rate experiment was carried out under the pressure of 0.1 MPa, and by comparing the concentration of BSA before and after the membrane filtration, the retention efficiency of the cellulose membrane was determined as follows,

$$R = \left(1 - \frac{c_1}{c_2}\right) \times 100\% \tag{2}$$

where R is the membrane retention rate (%),  $C_1$  is the feed concentration (mg/L), and  $C_2$  is the filtrate concentration (mg/L).

Membrane anti-fouling performance

From the BSA retention studies of the membrane, it was observed that the water flux of the membrane decreased as a result of protein adsorption on the surface of the membrane. To address this, the membrane was subjected to a 45-min washing process with deionized water. Subsequently, the water flux of the membrane was reevaluated under the same experimental conditions and steps as described in Eq. 1. Its membrane water flux recovery rate was calculated as follows,

$$FR = \frac{Q_{W2}}{Q_{W1}} \times 100\% \tag{3}$$

where FR is the water flux recovery percentage of the membrane (%) and  $Q_{W2}$  is the water flux after BSA filtration (LMH).

# Membrane antimicrobial properties

Using the disc diffusion method, the antibacterial ability of the produced composite membranes was qualitatively assessed. *Staphylococcus aureus* (*S. aureus*, Gram-positive strain, ATCC 6538) and *Escherichia coli* (*E. coli*, Gram-negative strain, ATCC 25922) were selected for testing. Initially, agar plates (Muller Hinton) were uniformly plated with bacterial suspensions. Furthermore, 6 mm-diameter membrane pieces were positioned on it. Then the agar plates were incubated at 37 °C for 24 h. In addition to taking pictures for documentation, the diameter of the inhibitory zone surrounding the substance was measured in millimeters and documented (Prerana *et al.* 2022).

### Heavy metal ions removal ability

The influence of several pivotal parameters on metal ion removal was examined. The parameters were Ag/UiO-66-NH<sub>2</sub> content (ranging from 0 to 1.5 wt%), pH levels (ranging from 2 to 7), contact duration (varying between 5 and 90 min), initial metal ion concentrations (ranging from 20 to 1000 mg/L), and temperature (ranging from 25 to 45 °C). The pH of the solution was adjusted using H<sub>2</sub>SO<sub>4</sub> and NaOH. The Ag/UiO-66-NH<sub>2</sub>, which had been previously synthesized, was employed as an adsorbent for metal ion adsorption. The adsorption capacity of Ag/UiO-66-NH<sub>2</sub>@BCM for metal ions was calculated as follows,

$$Q = \frac{(C_1 - C_2)V}{M} \tag{4}$$

where  $C_1$  (mg/L) and  $C_2$  (mg/L) represent the initial and final concentrations of metal ions, respectively, V is the volume (L), and M is the mass of MOF adsorbent (g).

# **RESULTS AND DISCUSSION**

# Surface Morphology of Ag/UiO-66-NH2@BCM

The morphology of the top surface, cross-section, and sponge-like pore structure of the fabricated mixed matrix membranes were examined using FESEM. A large number of pores were observed on the surface of the membrane, as shown in Fig. 3. The cellulose membrane, being hydrophilic, rapidly underwent liquid-liquid delamination with water during the water coagulation process, resulting in the formation of several pores. Upon the incorporation of 1 wt% Ag/UiO-66-NH<sub>2</sub> particles, a reduction of the pores was observed, rendering the membrane surface dense without any agglomeration, as shown in Fig. 3(a-b). This feature indicates that the nanoparticles were uniformly dispersed within the cellulose membrane, serving to fill the pores within the cellulose matrix. Figure 3(c-d) demonstrates that the Ag/UiO-66-NH<sub>2</sub>@BCM structure featured a distinct reticular pattern. This modification imparted a high level of hydrophilicity to the cellulose membrane and enhanced its overall stability, which is attributed to the interaction between cellulose and Ag/UiO-66-NH<sub>2</sub> particles.

To gain insights into the elemental composition of Ag/UiO-66-NH<sub>2</sub>@BCM, EDS analysis was conducted, as shown in Fig. 4(a). The detection of carbon (C) and oxygen (O) elements confirms the chemical composition of cellulose. Furthermore, the presence of

zirconium (Zr) and silver (Ag) elements implies the successful dispersion of Ag/UiO-66-NH<sub>2</sub> within the casting solution of the NMMO solvent system, with subsequent embedding in the cellulose membrane, resulting in improved membrane structure. These findings affirm the effective dispersion and integration of Ag/UiO-66-NH<sub>2</sub> particles throughout the cellulose membrane preparation process. Consequently, the preparation method of Ag/UiO-66-NH<sub>2</sub>@BCM composites can be regarded as having substantial potential for the fabrication of high-performance cellulose membranes.

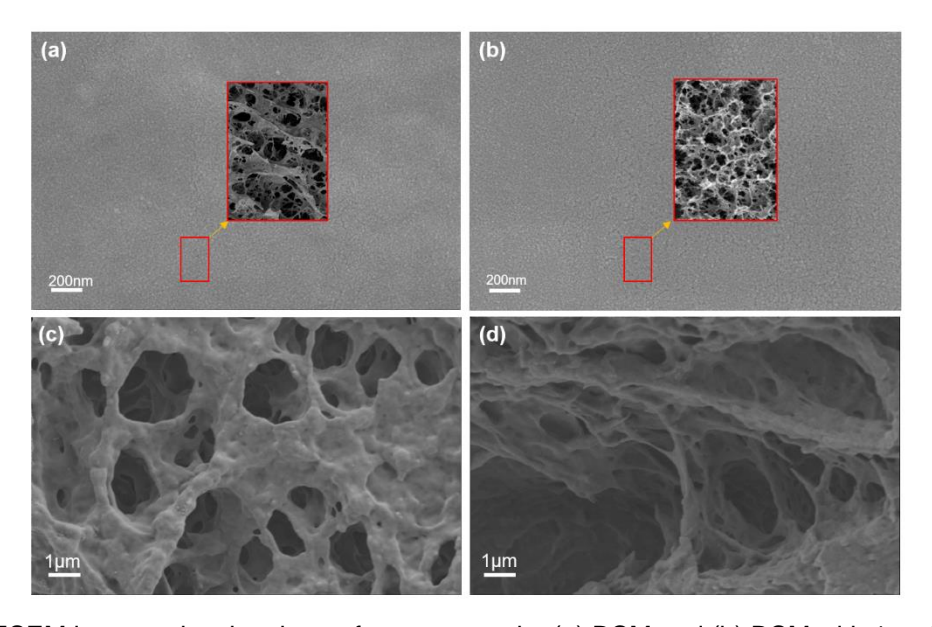


**Fig. 3.** FESEM images showing the surface topography (a) BCM and (b) BCM with 1 wt.% Ag/UiO-66-NH<sub>2</sub>. Cross-sectional morphology of (c) BCM and (d) BCM with 1 wt.% Ag/UiO-66-NH<sub>2</sub>

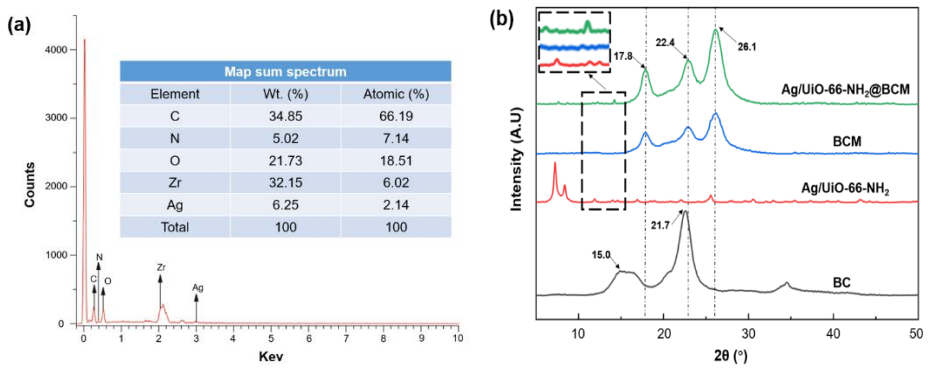


Fig. 4. EDS spectra of (a) 1 wt.% Ag/UiO-66-NH2@BCM. (b) XRD images of different samples

Figure 4(b) shows the results from the XRD analysis of BC, Ag/UiO-66-NH<sub>2</sub>, BCM, and Ag/UiO-66-NH<sub>2</sub>@BCM samples, where the crystalline structure of cellulose can be observed at the stronger diffraction peaks at  $2\theta$  of  $15.0^{\circ}$ ,  $17.8^{\circ}$ ,  $22.4^{\circ}$ , and  $26.1^{\circ}$ . The intensity trends of the diffraction peaks is suggestive of increased crystallinity of cellulose during the dissolution and regeneration process. This is ascribed to the opening of intra- and intermolecular hydrogen bonds in the cellulose molecules during the dissolution process, which leads to the disruption of the crystal structure of cellulose. In addition, the Ag/UiO-66-NH<sub>2</sub>@BCM samples showed significant peaks at higher  $2\theta$ , which could be attributed to the presence of Ag/UiO-66-NH<sub>2</sub> particles, which increased the

crystal structure of the samples. It is worth noting that the Ag/UiO-66-NH<sub>2</sub> particles were homogeneously dispersed in the BCM film. Therefore, the stability of the crystal structure of this composite is expected to be better than that of Ag/UiO-66-NH<sub>2</sub> particles alone. XRD analysis provides a better understanding of the crystal structures of BCM and Ag/UiO-66-NH<sub>2</sub>@BCM and lays the foundation for further investigation of their physical and chemical properties.

# Physicochemical Structure of the Ag/UiO-66-NH2@BCM

FT-IR and TG were used to detect the physicochemical properties of BC, BCM, and Ag/UiO-66-NH<sub>2</sub>@BCM samples. FT-IR analysis revealed that the characteristic peaks of BC, BCM, and Ag/UiO-66-NH<sub>2</sub>@BCM samples were similar, which indicates that the structure of cellulose and cellulose regeneration membranes had not changed, as shown in Fig. 5(a). Upon dissolution of cellulose in NMMO solvent, the macromolecular structure opened up, generating intramolecular as well as intermolecular hydrogen bonding, and -OH and -NH stretching vibrational intensity peaks appeared at 3322 cm<sup>-1</sup>. The presence of C-H elongation at 2900 cm<sup>-1</sup>, C=O elongation at 1652 cm<sup>-1</sup>, and C-O elongation vibrational peaks at 1060 cm<sup>-1</sup> in the graph confirms the presence of the cellulose component. In addition, the presence of C=O elongation at both 1630 cm<sup>-1</sup> and C-O elongation vibrational peaks at 1060 cm<sup>-1</sup> further confirms the presence of cellulose component (Ji et al. 2021). The positions of the Ag/UiO-66-NH<sub>2</sub>@BCM absorption peaks were similar to those of BCM, without any new absorption peaks in the FT-IR spectra. It can be inferred that the addition of Ag/UiO-66-NH2 did not change the structure of cellulose regeneration membrane. In addition, the positions of the characteristic peaks of Ag/UiO-66-NH<sub>2</sub> were slightly displaced, which might be due to the change of the stress in the membrane by the addition of nanoparticles, resulting in the contraction of the organic phase in the membrane (Liu et al. 2022).

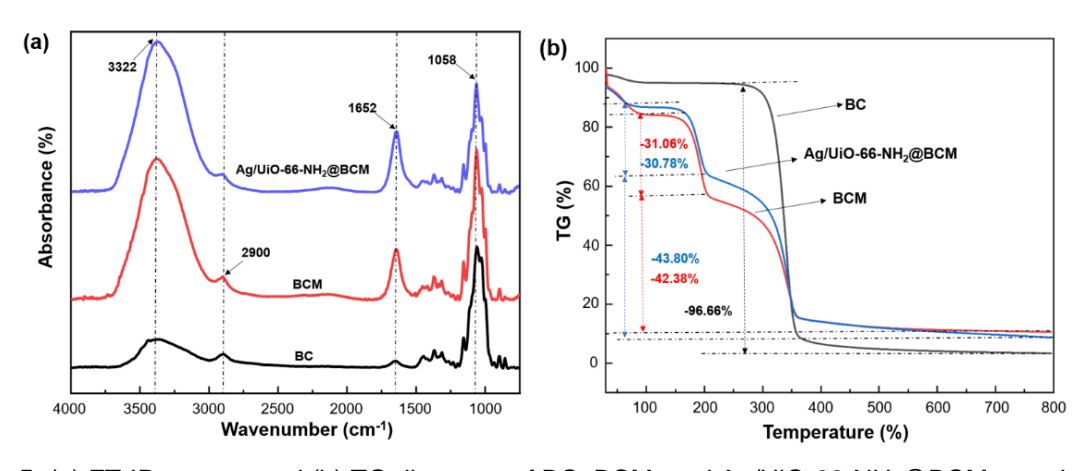


Fig. 5. (a) FT-IR spectra and (b) TG diagrams of BC, BCM, and Ag/UiO-66-NH<sub>2</sub>@BCM samples

TG analysis of the BC, BCM, and Ag/UiO-66-NH<sub>2</sub>@BCM samples revealed that water evaporated from the surfaces and a certain amount of degradation could be observed below 100 °C. The initial decomposition temperatures of BC, BCM, and Ag/UiO-66-NH<sub>2</sub>@BCM samples were 318.0 °C, 60.6 °C, and 58.0 °C, respectively. A mass change of 96.7% was observed for BC, which was attributed to the decomposition of the cellulose molecular backbone. Compared to BC, the thermal stability of BCM was slightly lower, which might be due to the degradation of cellulose during dissolution and regeneration.

From the TG curves it was deduced that Ag/UiO-66-NH<sub>2</sub>@BCM has more residue remaining than BCM when the thermal decomposition is completed. Combined with XRD analysis, a certain force exists between Ag/UiO-66-NH<sub>2</sub>@BCM particles and cellulose polymer, which changes the stress distribution of cellulose regenerated membrane (Liu *et al.* 2022a). In addition, nano-Ag/UiO-66-NH<sub>2</sub> is a stable thermal material, which imparts a higher degree of thermal stability to Ag/UiO-66-NH<sub>2</sub>@BCM compared to BCM.

# Water Permeability and Ultrafiltration

Water flux and BSA retention are crucial metrics utilized in the evaluation of UF membranes (Liu *et al.* 2022b). Water flux represents the capacity of the membrane to transmit water molecules, while BSA retention rate characterizes its efficacy in blocking larger molecules. Introduction of Ag/UiO-66-NH<sub>2</sub> resulted in a 17.5% increase in the pure water flux for M2 and a 31.4% increase for M3 compared to M0, as shown in Fig. 6(a). This suggests that the incorporation of Ag/UiO-66-NH<sub>2</sub> enhanced the water permeability of the membrane. Additionally, the water flux showed a positive correlation with the quantity of Ag/UiO-66-NH<sub>2</sub> added to the casting solution. This feature can be attributed to the hydrophilic additives, which influence the kinetics of the membrane solution, expedite solvent-nonsolvent separation, and contribute to the formation of a more porous structure with larger pore sizes (Zhang *et al.* 2023). Consequently, this enhanced pore structure not only provided additional pathways for water molecule permeation but also reduces resistance during transport. Additionally, the hydrophilic additives enhanced the surface hydrophilicity of the membrane, attracting more water molecules to the membrane pores, thereby further improving water permeability.

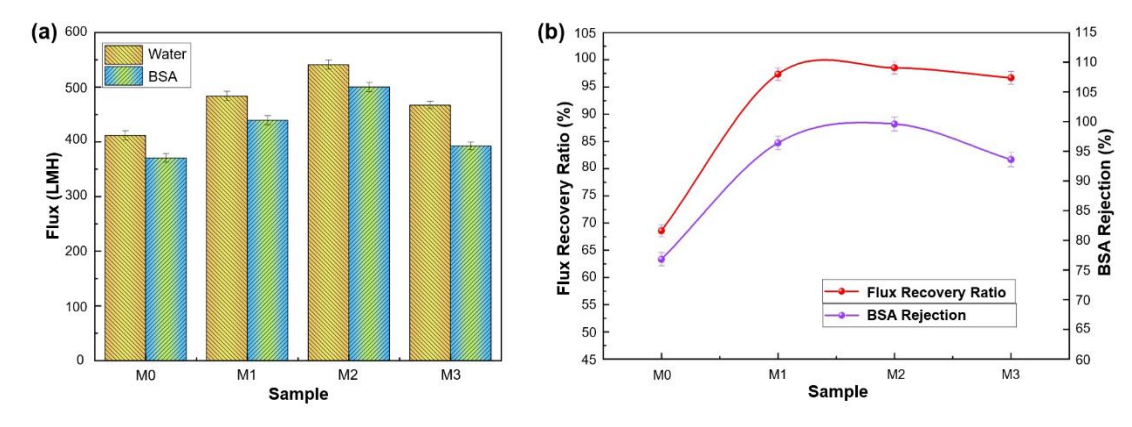


**Fig. 6.** Properties of composite membranes with different additives. (a) Water flux and BSA flux. (b) BSA retention rate and membrane flux recovery rate

Although the protein flux through all membranes was lower than that of water, it exhibited a pattern that was consistent with pure water flux variation based on the additive dosage, as shown in Fig. 6(a). The protein flux of the M2 membrane reached 500.16 LMH, which corresponded to a 35.0% increase compared to M0. This enhancement upon the of addition of Ag/UiO-66-NH<sub>2</sub> highlights the barrier effect of UF membranes against larger molecules and is attributed to the more uniform distribution of pore sizes in the membrane after the introduction of Ag/UiO-66-NH<sub>2</sub> (Ma *et al.* 2022). The optimized pore size distribution enhanced the capacity of the membrane to retain larger molecules. Figure 6(b) shows the BSA retention of the composite UF membrane. The pure BC membrane exhibited a retention efficiency of 76.8%, while the BSA rejection of the M3 membrane

increased to 89.1%, possibly due to increased pore size. With the inclusion of Ag/UiO-66-NH<sub>2</sub>, the retention percentage of the composite membrane increased, with M2 achieving the highest retention of 99.6%. This is primarily due to the more uniform dispersion of Ag/UiO-66-NH<sub>2</sub> in the casting solution, resulting in channels of consistent sizes. This not only enhances pure water flux but also ensures a higher BSA interception rate (Shen *et al.* 2022). The decrease in BSA retention to 93.6% for the M3 membrane may be attributed to the enlarged pore size. Additionally, the introduction of -NH<sub>2</sub> from Ag/UiO-66-NH<sub>2</sub> into the membrane mixture imparts a stronger negative charge, preventing protein molecules from contacting the membrane surface (Liang *et al.* 2020).

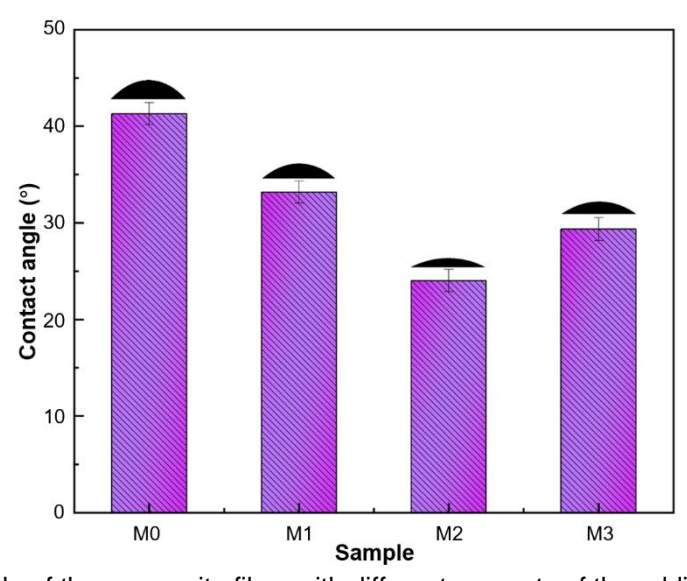


Fig. 7. Contact angle of the composite films with different amounts of the additive

The hydrophilicity of the blended films was assessed through water contact angle measurements, as shown in Fig. 7. The contact angle for M0 was the highest at 41.3°, which was consistent with the inherent hydrophilic nature of BC. As Ag/UiO-66-NH<sub>2</sub> was introduced, the contact angle of the blended membrane decreased. For the M2 sample with 1 wt.% Ag/UiO-66-NH<sub>2</sub> loading, the water contact angle dropped to 24.0°. This reduction was attributed to the incorporation of hydrophilic functional groups (-OH and -NH<sub>2</sub>) from Ag/UiO-66-NH<sub>2</sub>, which enhanced the chemical properties of the membrane surface (Peng *et al.* 2023). A hydrophilic membrane surface exhibits a strong affinity for water molecules, facilitating their penetration into the membrane matrix, thus resulting in increased water flux. Modification with hydrophilic functional groups effectively enhances membrane hydrophilicity. In M2, the presence of hydrophilic functional groups from Ag/UiO-66-NH<sub>2</sub> notably improved the hydrophilicity of the membrane surface, leading to the minimum contact angle and higher water flux. These findings demonstrate the tunability of the hydrophilic properties of the hybrid membrane through surface chemistry alterations, offering a novel approach for crafting UF membranes with desired characteristics.

# Ag/UiO-66-NH<sub>2</sub>@BCM Anti-fouling Property

The anti-contamination performance of the prepared UF membranes was evaluated using BSA solution (1 g/L) and quantified by FR index. The results showed that the UF membranes modified with hydrophilic fillers had high fouling resistance and reusability. Figure 6(b) demonstrates the FR values of various UF membranes examined. It can be seen

that the FR value of M0 was only 68.6%, which is ascribed to the rougher surface of this membrane that pollutants can easily adhere to. After the modification of hydrophilic filler, the FR values of all membranes were improved. Among them, M2 had the highest FR value of 98.5%, which was 42.0% higher than that of M1. This indicates that hydrophilic filler modification can significantly improve the anti-pollution ability of UF membranes, resulting in longer service life and better performance stability.

# Ag/UiO-66-NH2@BCM Antibacterial Properties

Based on the previous research, it was concluded that the M2 membrane exhibited the most superior comprehensive performance. Therefore, subsequent experiments were conducted using the M2 composite membrane scheme. The antibacterial performance against *E. coli* and *S. aureus* contamination was assessed using the prepared membranes, as shown in Fig. 8 and Table 2.

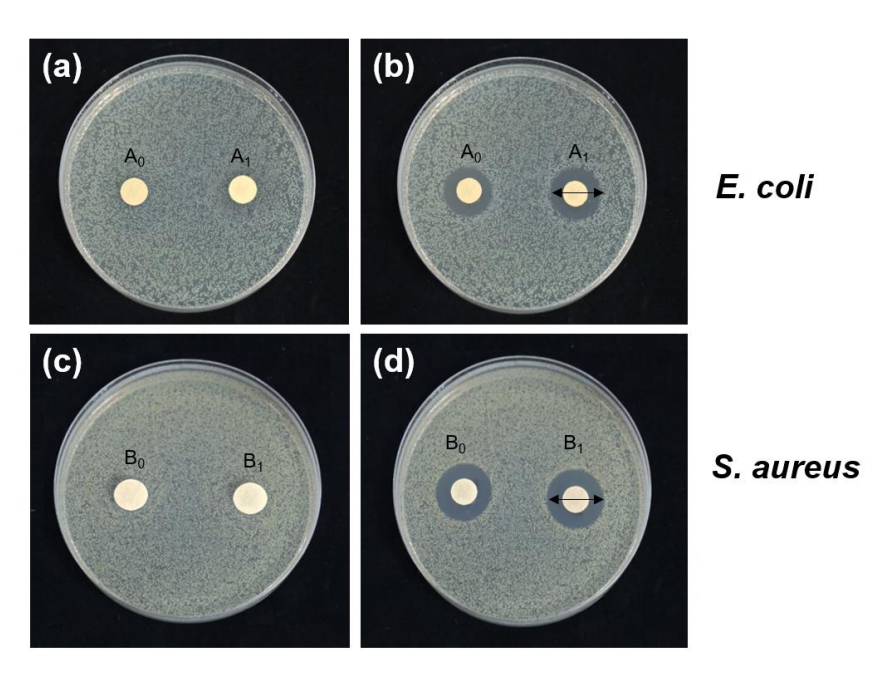


Fig. 8. Inhibition zone of Ag/UiO-66-NH2@BCM on (a) (b) E. coli and (c) (d) S. aureus

**Table 2.** Inhibition Circle Diameter D (mm) for Ag/UiO-66-NH<sub>2</sub>@BCM

Membrane code	A0	A1	B0	B1
Diameter(mm)	E.	coli	S. aureus	
Diameter(mm)	7.055	7.133	8.416	8.797

The maximal antibacterial zone diameters of Ag/UiO-66-NH<sub>2</sub>@BCM against *E. coli* and *S. aureus* were 7.13 and 8.8 mm, respectively. Ag/UiO-66-NH<sub>2</sub>@BCM demonstrated greater efficacy against *S. aureus* than against *E. coli*, as previously reported (Tian *et al.* 2022). A complex mechanism is involved in the antibacterial action of Ag/UiO-66-NH<sub>2</sub>, where the absorption and release of silver ions acting as oxidizing agents results in the destruction of the organic component of the bacterial cell wall and subsequent microbial death (Hussein *et al.* 2020). Another proposed mechanism involves the active metal sites on the crystal surface of Ag/UiO-66-NH<sub>2</sub> altering the transmembrane potential of bacterial cells, making bacterial membrane proteins and fatty acids more susceptible to

oxidation, which results in bacterial inactivation (Ng *et al.* 2016). The crystal structure of MOF also contributes to its enhanced antimicrobial activity. These results affirm the potential of Ag/UiO-66-NH<sub>2</sub>@BCM as an effective *in vivo* biocidal material.

Upon examination of the capacity of Ag/UiO-66-NH<sub>2</sub>@BCM for prolonged bactericidal action, a study investigating its sustained Ag<sup>+</sup> release in a simulated aqueous environment over 30 days was undertaken. Figure 9 illustrates a stable release rate of approximately 0.25  $\mu$ g L<sup>-1</sup> day<sup>-1</sup>, indicative of secure Ag<sup>+</sup> incorporation and consistent bactericidal performance. Notably, the total Ag<sup>+</sup> release remained far below the permitted level for drinking water (0.05 mg/L), ensuring environmental safety and applicability. These findings highlight the potential of Ag/UiO-66-NH<sub>2</sub>@BCM as an effective, longlasting, and environmentally friendly antimicrobial membrane.

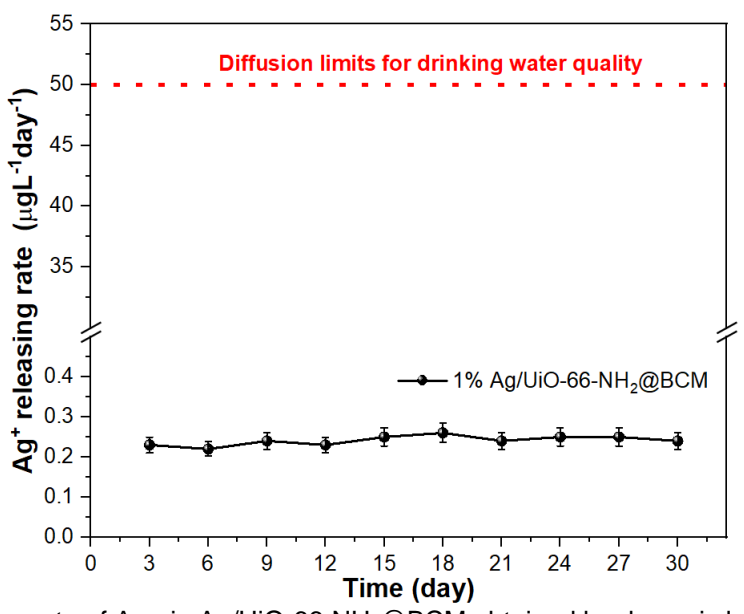


Fig. 9. The release rate of Ag+ in Ag/UiO-66-NH2@BCM obtained by dynamic leaching

#### **Heavy Metal Ions Removal Performance**

Performance analysis of Ag/UiO-66-NH<sub>2</sub>@BCM showed that the MOF content had an important effect on the efficiency of metal ion removal. The composite membrane exhibited the maximum removal of metal ions when the Ag/UiO-66-NH<sub>2</sub> content was 1.0 wt.%, as shown in Fig. 10. This is because the MOF has a larger surface area in the composite membrane, which can provide more adsorption sites.

The chelation of MOF functional groups with metal ions can enhance the interaction between metal ions and MOF, thus increasing the removal rate of metal ions. Compared with samples with other concentrations, the composite membrane with 1.0 wt.% of MOF had a higher removal rate. Loading Ag/UiO-66-NH<sub>2</sub> into cellulose membranes not only improved the mechanical strength and stability of the composite membranes, but also the chelation of MOF functional groups improved the removal of metal ions. These results demonstrate that the removal performance of Ag/UiO-66-NH<sub>2</sub>@BCM for metal ions in water is very promising.

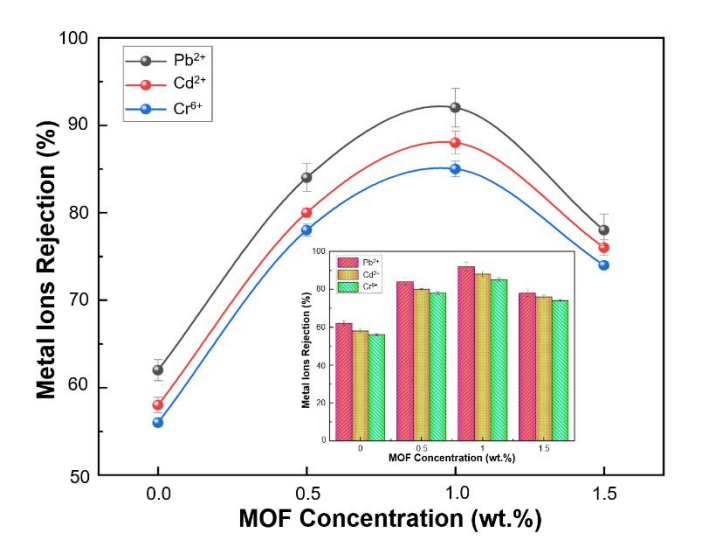


Fig. 10. Influence of MOF content on removal rate of metal ions

The impact of different initial concentrations of metal ions on the removal performance of Ag/UiO-66-NH<sub>2</sub>@BCM was ascertained through removal experiments. The removal amount of metal ions steadily increased with increasing metal ion concentration in the 5 to 50 mg/L range, as shown in Fig. 11. This phenomenon can be attributed to the acceleration of metal ion diffusion at higher concentrations, resulting in an enhanced driving force and facilitating metal ion removal. This trend aligns with Fick's law of diffusion, which states that the diffusion rate is proportional to the concentration gradient, meaning that the greater the concentration difference, the faster the diffusion rate (Binish *et al.* 2022).

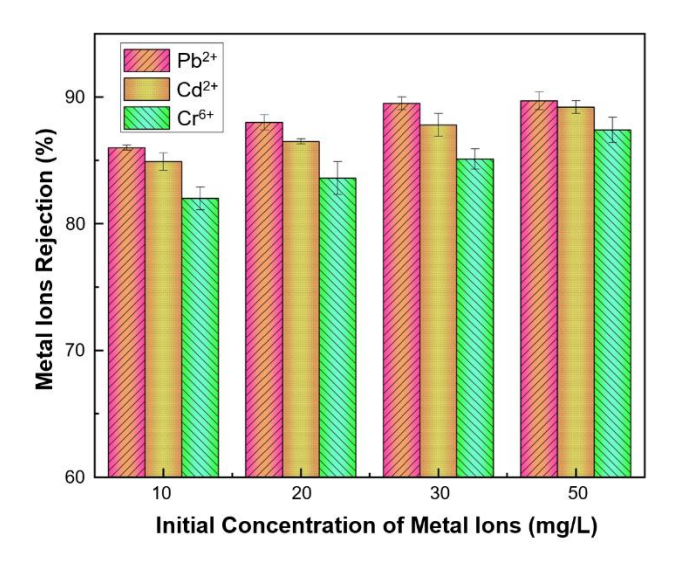
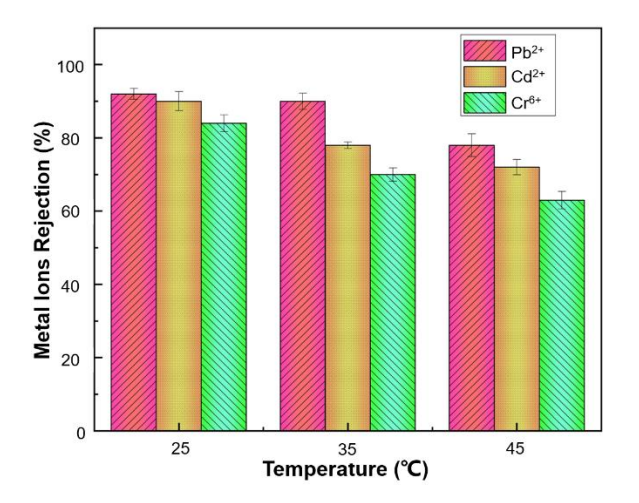


Fig. 11. Influence of initial concentration of metal ions on the ion removal rate

The influence of temperature on flux and metal ion removal is shown in Fig. 12. Metal ion removal decreased as the temperature increased from 25 to 45 °C. This can be attributed to a reduction in the doping of metal ions in the membrane pores at higher temperatures, leading to a gradual decline in the metal ion removal rate. Additionally, temperature-induced changes in membrane pore size may impact the adsorption and

diffusion processes of metal ions, further affecting the efficiency of metal ion removal.

The performance of Ag/UiO-66-NH<sub>2</sub>@BCM for the removal of heavy metals for 24 h was investigated, and the results are shown in Fig. 13. The removal performance of the composite membrane for metal ions was found to remain constant for 18 h, beyond which the removal performance showed a significant decline. Thus, the removal performance of the composite membrane is affected by long filtration times. The surface pores and internal pores of the composite membrane are responsible for ion removal (Bashir *et al.* 2019). When the Ag/UiO-66-NH<sub>2</sub>@BCM pores were saturated, the shedding of metal ions decreased with time. Although the composite membrane has a good removal effect for a short period of time, its removal performance is limited and degraded by factors such as pore saturation. Therefore, the composite membrane needs to be replaced or cleaned periodically to maintain optimal performance. In addition, the pore structure and saturation of the composite membrane should be considered in the preparation of the composite membrane to achieve better removal effect and stability.



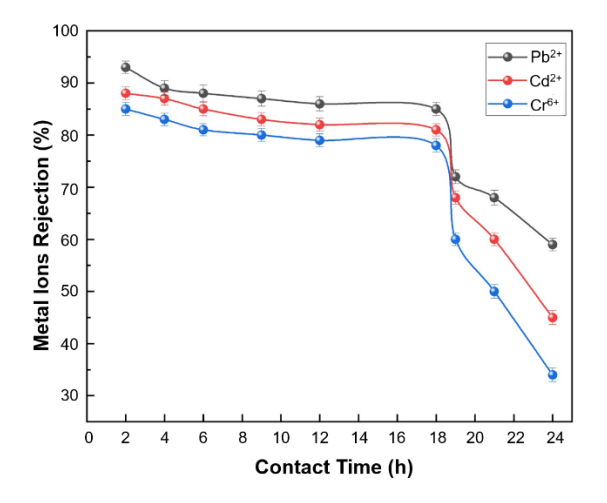


**Fig. 12.** Effect of temperature on removal rate of metal ions

Fig. 13. Influence of contact time on removal rate of metal ions

#### CONCLUSIONS

- 1. In this study, cellulose ultrafiltration membranes were fabricated using the phase transformation method. High-performance composite ultrafiltration membranes were developed by introducing the metal-organic framework Ag/UiO-66-NH<sub>2</sub> into the bamboo cellulose (BC) casting solution for blending. Incorporation of Ag/UiO-66-NH<sub>2</sub> enhanced the ultrafiltration performance of all membranes in terms of pore structure, permeability, and antifouling characteristics. Notably, the M2 membrane demonstrated the best performance with a pure water flux of 541.12 LMH and a BSA retention rate of 99.6%, accompanied by an flux recovery (FR) value of 97.4%.
- 2. In addition, the membranes blended with Ag/UiO-66-NH<sub>2</sub> also possessed good antibacterial properties, effectively inhibiting the growth of both *E. coli* and *S. aureus*. This indicates that the addition of Ag/UiO-66-NH<sub>2</sub> can improve the antimicrobial performance of the membranes, which enables new applications in biomedical engineering and other fields. The removal of Pb<sup>2+</sup>, Cd<sup>2+</sup>, and Cr<sup>6+</sup> ions by Ag/UiO-66-NH<sub>2</sub>@BCM showed that the order of the removal ability of the nanofibers for metal

ions was  $Pb^{2+} > Cd^{2+} > Cr^{6+}$ . The high reusability of the synthesized Ag/UiO-66-NH<sub>2</sub> adsorbent indicates that the MOF material has high potential for the removal of heavy metal ions from aqueous solution.

#### **ACKNOWLEDGMENTS**

This research is financially supported by the General project of Fujian Provincial Natural Science Foundation (2022J01922, 2023J01935), the major special projects of Fujian Province (2023YZ038009), and the Science and Technology Project of Fujian Provincial Department of Natural Resources (KY-090000-04-2024-025).

#### REFERENCES CITED

- Ajibade, T. F., Tian, H., Hassan Lasisi, K., Xue, Q., Yao, W., and Zhang, K. (2021). "Multifunctional PAN UF membrane modified with 3D-MXene/O-MWCNT nanostructures for the removal of complex oil and dyes from industrial wastewater," *Separation and Purification Technology* 275, article 119135. DOI: 10.1016/j.seppur.2021.119135
- Aloulou, H., Aloulou, W., Daramola, M. O., and Ben Amar, R. (2021). "Silane-grafted sand membrane for the treatment of oily wastewater *via* air gap membrane distillation: Study of the efficiency in comparison with microfiltration and ultrafiltration ceramic membranes," *Materials Chemistry and Physics* 261, article 124186. DOI: 10.1016/j.matchemphys.2020.124186
- Awad, E. S., Sabirova, T. M., Tretyakova, N. A., Alsalhy, Q. F., Figoli, A., and Salih, I. K. (2021). "A mini-review of enhancing ultrafiltration membranes (UF) for wastewater treatment: Performance and stability," *ChemEngineering* 5(3), article 34. DOI: 10.3390/chemengineering5030034
- Bashir, A., Malik, L. A., Ahad, S., Manzoor, T., Bhat, M. A., Dar, G. N., and Pandith, A. H. (2019). "Removal of heavy metal ions from aqueous system by ion-exchange and biosorption methods," *Environmental Chemistry Letters* 17 (2), 729-754. DOI: 10.1007/s10311-018-00828-y
- Binish, C. J., Vijayasankar, A. V., and Shamaan, M. P. (2022). "Synthesis and characterization of poly-vinyl alcohol-alumina composite film: An efficient adsorbent for the removal of chromium (VI) from water," *Materials Today: Proceedings* 62(8), 5182-5188. DOI: 10.1016/j.matpr.2022.02.629
- Chai, S., Xie, Y., and Yang, L. (2022). "Antibacterial applications of elemental nanomaterials," *Current Opinion in Solid State and Materials Science* 26(6), article 101043. DOI: 10.1016/j.cossms.2022.101043
- Fatima, F., Du, H., and Kommalapati, R. R. (2021). "Treatment of poultry slaughterhouse wastewater with membrane technologies: A review," *Water* 13 (14), article 1905. DOI: 10.3390/w13141905
- Geng, C., Fan, L. A., Niu, H., Liu, L., Zhao, F., Zhang, J., Dong, H., and Yu, S. (2021). "Improved anti-organic fouling and antibacterial properties of PVDF ultrafiltration membrane by one-step grafting imidazole-functionalized graphene oxide," *Materials Science and Engineering C* 131, article 112517. DOI: 10.1016/j.msec.2021.112517
- Huang, X., Tian, F., Chen, G., Wang, F., Weng, R., and Xi, B. (2021). "Preparation and

- characterization of regenerated cellulose membrane blended with ZrO(2) nanoparticles," *Membranes (Basel)* 12(1). DOI: 10.3390/membranes12010042
- Hussein, J., El-Naggar, M. E., Fouda, M. M. G., Morsy, O. M., Ajarem, J. S., Almalki, A., M., Allam, A. A., and Mekawi, E. M. (2020). "The efficiency of blackberry loaded AgNPs, AuNPs and Ag@AuNPs mediated pectin in the treatment of cisplatin-induced cardiotoxicity in experimental rats," *International Journal of Biological Macromolecules* 159, 1084-1093. DOI: 10.1016/j.ijbiomac.2020.05.115
- Janmohammadi, M., Nazemi, Z., Salehi, A. O. M., Seyfoori, A., John, J. V., Nourbakhsh, M. S., and Akbari, M. (2023). "Cellulose-based composite scaffolds for bone tissue engineering and localized drug delivery," *Bioactive Materials* 20, 137-163. DOI: 10.1016/j.bioactmat.2022.05.018
- Jawad, J., Hawari, A. H., and Javaid Zaidi, S. (2021). "Artificial neural network modeling of wastewater treatment and desalination using membrane processes: A review," *Chemical Engineering Journal* 419, article 129540. DOI: 10.1016/j.cej.2021.129540
- Ji, L., Zhang, F., Zhu, L., and Jiang, J. (2021). "An in-situ fabrication of bamboo bacterial cellulose/sodium alginate nanocomposite hydrogels as carrier materials for controlled protein drug delivery," *International Journal of Biological Macromolecule* 170, 459-468. DOI: 10.1016/j.ijbiomac.2020.12.139
- Kaur, R., Goyat, R., Singh, J., Umar, A., Chaudhry, V., and Akbar, S.(2022). "An overview of membrane distillation technology: One of the perfect fighters for desalination," *Engineered Science*. DOI: 10.30919/es8d771
- Khanzada, N. K., Farid, M. U., Kharraz, J. A., Choi, J., Tang, C. Y., Nghiem, L. D., Jang, A., and An, A. K. (2020). "Removal of organic micropollutants using advanced membrane-based water and wastewater treatment: A review," *Journal of Membrane Science* 598, article 117672. DOI: 10.1016/j.memsci.2019.117672
- Kim, D.-Y., Saratale, R. G., Shinde, S., Syed, A., Ameen, F., and Ghodake, G. (2018). "Green synthesis of silver nanoparticles using *Laminaria japonica* extract: Characterization and seedling growth assessment," *Journal of Cleaner Production* 172, 2910-2918. DOI: 10.1016/j.jclepro.2017.11.123
- Liang, Y., Ma, H., Taha, A. A., and Hsiao, B. S. (2020). "High-flux anti-fouling nanofibrous composite ultrafiltration membranes containing negatively charged water channels," *Journal of Membrane Science* 612, article 118382. DOI: 10.1016/j.memsci.2020.118382
- Liu, G., Ji, C., Li, J., and Pan, X. (2022a). "Facile preparation and properties of superhydrophobic nanocellulose membrane," *Arabian Journal of Chemistry* 15(8), article 103964. DOI: 10.1016/j.arabjc.2022.103964
- Liu, Y., Liu, Y., Li, X., Qian, Y., Lv, L., and Wang, Y. (2022b). "Fabrication and research of Mg(OH)<sub>2</sub>/PCL/PVP nanofiber membranes loaded by antibacterial and biosafe Mg(OH)<sub>2</sub> nanoparticles," *Polymer Testing* 112, article 107635. DOI: 10.1016/j.polymertesting.2022.107635
- Liu, Z., Qiang, R., Lin, L., Deng, X., Yang, X., Zhao, K., Yang, J., Li, X., Ma, W., and Xu, M. (2022). "Thermally modified polyimide/SiO<sub>2</sub> nanofiltration membrane with high permeance and selectivity for efficient dye/salt separation," *Journal of Membrane Science* 658, article 120747. DOI: 10.1016/j.memsci.2022.120747
- Ma, C., Nikiforov, A., Gromov M, Ostrikov, K., Geyter, N. D., and Morent, R. (2022). "Plasma-aerosol-assisted surface engineering for scalable oil/water membrane separation," *Applied Surface Science* 606, article 154807. DOI:

- 10.1016/j.apsusc.2022.154807
- Miao, Q., Jiang, L., Yang, J., Hu, T., Shan, S., Su, H., and Wu, F. (2022). "MOF/hydrogel composite-based adsorbents for water treatment: A review," *Journal of Water Process Engineering* 50, article 103348. DOI: 10.1016/j.jwpe.2022.103348
- Musarurwa, H., and Tavengwa, N. T. (2022). "Smart metal-organic framework (MOF) composites and their applications in environmental remediation," *Materials Today Communications* 33, article 104823. DOI: 10.1016/j.mtcomm.2022.104823
- Ng, T. W., Zhang, L., Liu, J., Huang, G., Wang, W., and Wong, P. K. (2016). "Visible-light-driven photocatalytic inactivation of *Escherichia coli* by magnetic Fe<sub>2</sub>O<sub>3</sub>-AgBr," *Water Research* 90, 111-118. DOI: 10.1016/j.watres.2015.12.022
- Peng, R., Zhang, S., Yao, Y., Wang, J., Zhu, X., Jiang, R., Zhang, W., and Wang C. (2023). "MOFs meet electrospinning: New opportunities for water treatment," *Chemical Engineering Journal* 453, article 139669. DOI: 10.1016/j.cej.2022.139669
- Peydayesh, M., and Mezzenga, R. (2021). "Protein nanofibrils for next generation sustainable water purification," *Nature Communications* 12(1), article 3248. DOI: 10.1038/s41467-021-23388-2
- Prerana, S., Surabhi, A., Mangal, S. R., and Shahi, V. K. (2022). "Cross-linked anion-exchange membrane with side-chain grafted multi-cationic spacer for electrodialysis: Imparting dual anti-fouling and anti-bacterial characteristics," *Journal of Membrane Science* 660, article 120871. DOI: 10.1016/j.memsci.2022.120871
- Ruan, W., Liu, H., Wu, H., Qi, Y., Zhou, M., Zhou, C., Zhang, Z., and Yang, H. (2022). "Fabrication of Uio-66-NH2 with 4,6-Diamino-2-mercaptopyrimidine facilitate the removal of Pb<sup>2+</sup> in aqueous medium: Nitrogen and sulfur act as the main adsorption sites," *Fuel Processing Technology* 236, article 107431. DOI: 10.1016/j.fuproc.2022.107431
- Shen, H., Cui, C., Wang, Z., Wang, Y., Zhu, L., Chen, W., Liu Q., Zhang, Z., Wang, H., and Yang, K. (2022). "Poly(arylene ether ketone) with carboxyl groups ultrafiltration membrane for enhanced permeability and anti-fouling performance," *Separation and Purification Technology* 281, article 119885. DOI: 10.1016/j.seppur.2021.119885
- Tarpeh, W. A., and Chen, X. (2021). "Making wastewater obsolete: Selective separations to enable circular water treatment," *Environmental Science and Ecotechnology* 5, article 100078. DOI: 10.1016/j.ese.2021.100078
- Tian, F., Weng, R., Huang, X., Chen, G., and Huang, Z. (2022). "Fabrication of silver-doped UiO-66-NH2 and characterization of antibacterial materials," *Coatings* 2022, 12(12), article 1939. DOI: 10.3390/coatings12121939
- Weng, R., Tian, F., Huang, X., Ni, L., and Xi, B. (2021). "Preparation of cellulose nanofiltration membranes and their removal of typical pollutants from drinking water," *Water Supply* 21(8), 4355-4368. DOI: 10.2166/ws.2021.183
- Weng, R., Tian, F., Huang, X., and Chen, G. (2022). "IP–ZrO<sub>2</sub>/BC nanofiltration membranes: Preparation and properties," *Coatings* 12(12). DOI: 10.3390/coatings12121823
- Weng, X., Ji, Y., Ma, R., Zhao, F., An, Q., and Gao, C. (2016). "Superhydrophilic and antibacterial zwitterionic polyamide nanofiltration membranes for antibiotics separation," *Journal of Membrane Science* 510, 122-130. DOI: 10.1016/j.memsci.2016.02.070.
- Wu, Y., Chen, M., Lee, H. J., M, A. G., Zhang, N., and de Lannoy, C. F. (2022). "Nanocomposite polymeric membranes for organic micropollutant removal: A critical review," *ACS ES&T Engineering* 2 (9), 1574-1598. DOI:

- 10.1021/acsestengg.2c00201
- Yamane, C., Aoyagi, T., Ago, M., Sato, K., Okajima, K., and Takahashi, T. (2006). "Two different surface properties of regenerated cellulose due to structural anisotropy," *Polym. J.* 38(8), 819-826. DOI: 10.1295/polymj.PJ2005187
- Zhang, J., Zhang, F., Fang, W., and Jin, J. (2023). "Membrane wettability manipulation via mixed-dimensional heterostructured surface towards highly efficient oil-in-water emulsion separation," *Journal of Membrane Science* 672, article 121472. DOI: 10.1016/j.memsci.2023.121472
- Zhang, X., Liu, M., and Han, R. (2021). "Adsorption of phosphate on UiO-66-NH<sub>2</sub> prepared by a green synthesis method," *Journal of Environmental Chemical Engineering* 9(6), article 106672. DOI: 10.1016/j.jece.2021.106672
- Zhang, G., Zhou, M., Xu, Z., Jiang, C., Shen, C., and Meng, Q. (2019). "Guanidyl-functionalized graphene/polysulfone mixed matrix ultrafiltration membrane with superior permselective, antifouling and antibacterial properties for water treatment," *Journal of Colloid Interface Science* 540, 295-305. DOI: 10.1016/j.jcis.2019.01.050
- Zhang, J., Xu, Y. N., Chen, S., Li, J., Han, W., Sun, X., Wu, D., Hu, Z., and Wang, L. (2018). "Enhanced antifouling and antibacterial properties of poly (ether sulfone) membrane modified through blending with sulfonated poly (aryl ether sulfone) and copper nanoparticles," *Applied Surface Science* 434, 806-815. DOI: 10.1016/j.apsusc.2017.11.007
- Zhang, X. (2022). "Selective separation membranes for fractionating organics and salts for industrial wastewater treatment: Design strategies and process assessment," *Journal of Membrane Science* 643, article 120052. DOI: 10.1016/j.memsci.2021.120052
- Zhao, X. Q., Wahid, F., Cui, J. X., Wang, Y. Y., and Zhong, C. (2021). "Cellulose-based special wetting materials for oil/water separation: A review," *International Journal of Biological Macromolecules* 185, 890-906. DOI: 10.1016/j.ijbiomac.2021.06.167
- Zou, P., Yao, J., Cui, Y. N., Zhao, T., Che, J., Yang, M., Li, Z., and Gao, C. (2022). "Advances in cellulose-based hydrogels for biomedical engineering: A review summary," *Gels* 8(6), article 364. DOI: 10.3390/gels8060364

Article submitted: July 20, 2024; Peer review completed: September 14, 2024; Revised version received: September 15, 2024; Accepted: September 22, 2024; Published: October 10, 2024.

DOI: 10.15376/biores.19.4.8988-9006